

## CONVECTIVE HEAT TRANSFER IN A MICROPOLAR FLUID OVER AN UNSTEADY STRETCHING SURFACE

K.V. PRASAD\* and H. VAIDYA  
Department of Mathematics, VSK University  
Vinayaka Nagar, Bellary-583 105, Karnataka, INDIA  
E-mail: prasadkv2007@gmail.com

K. VAJRVELU  
Department of Mathematics  
Department of Mechanical, Materials and Aerospace Engineering  
University of Central Florida  
Orlando, FL 32816, USA

An unsteady boundary layer free convective flow and heat transfer of a viscous incompressible, micropolar fluid over a vertical stretching sheet is investigated. The stretching velocity is assumed to vary linearly with the distance along the sheet. Two equal and opposite forces are impulsively applied along the  $x$ -axis so that the sheet is stretched, keeping the origin fixed in the micropolar fluid. The transformed highly non-linear boundary layer equations are solved numerically by an implicit finite difference scheme for the transient, state from the initial to the final steady-state. To validate the numerical method, comparisons are made with the available results in the literature for some special cases and the results are found to be in good agreement. The obtained numerical results are analyzed graphically for the velocity, the microrotation, and the temperature distribution; whereas the skin friction, the couple stress coefficient and the Nusselt number are tabulated for different values of the pertinent parameters. Results exhibit a drag reduction and an increase in the surface heat transfer rate in the micropolar fluid flow compared to the Newtonian fluid flow.

**Key words:** unsteady flow, microrotation, heat transfer, skin friction, Nusselt number, Keller-box method.

### 1. Introduction

The analysis of convective flow and heat transfer over a vertical stretching sheet has gained interest due to its various applications to engineering/industrial disciplines. Examples are numerous and they include the aerodynamic extrusion of plastic sheets, the boundary layer along a liquid film in condensation processes, paper production, glass blowing, metal spinning and drawing plastic films. Since the process of continuous stretching depends on unidirectional orientation the quality of the final product considerably depends on the flow and heat transfer mechanism. In particular, the analysis of momentum and thermal transport within the fluid on a continuously stretching surface is important for gaining some fundamental understanding of such processes. Crane [1] is the first among the others to study such a flow caused by an elastic sheet moving in its own plane with a velocity varying linearly with the distance from a fixed point. Since then heat and mass transfer aspects have been studied by several authors (Gupta and Gupta [2], Chen and Char [3], Grubka and Bobba [4], Ali [5], Vajravelu [6], and Datta *et al.* [7]) for different physical situations: These studies deal with fluid flow and heat transfer in the absence of buoyancy force. However, in many practical situations the solid object moves in a quiescent fluid due to the fluid flow induced by the motion of the solid object and/or by the thermal buoyancy. Therefore the resulting flow and the thermal fields are determined by these two

---

\* To whom correspondence should be addressed

mechanisms; i.e., the surface motion and the thermal buoyancy. However, the buoyancy force effects were not considered in the afore-mentioned studies. Hence, the effects of thermal buoyancy on the flow and heat transfer over a stretching sheet were studied by several investigators (Chen and Strobel [8], Moutsoglou and Chen [9], Chen [10], Ingham [11], Ramachandran *et al.* [12], and Lee and Tsai [13], and Vajravelu [14]).

All the above investigators restrict their analyses to steady flow only. However, the flow and heat transfer problems are unsteady in nature, due to a sudden stretching of the flat sheet or due to the change in the temperature of the sheet. When the surface is impulsively stretched with certain velocity, the fluid flow is developed instantaneously. Elbashbeshy and Bazid [15] presented a similarity solution for the boundary layer equations, which describe the unsteady flow and heat transfer over a stretching sheet and extended by Abd El-Aziz [16] for some physically realistic phenomena. The unsteady flow over a stretching surface with a magnetic field in a rotating fluid was studied by Takhar and Nath [17]. The problem of heat transfer for the unsteady free convection flow over a continuous moving vertical surface has been investigated by Kumari *et al.* [18]. In all these studies the fluid is assumed to be Newtonian. However, most of the practical fluids are non-Newtonian, and it was first introduced by Eringen [19] and [20] as the theory of micropolar and thermo-micropolar fluids. This theory can be used to describe the behavior of fluids in many practical applications. These applications include the mathematical model for polymeric fluids, colloidal fluids, fluids with suspensions, liquid crystal, animal blood and exotic lubricants: For these fluids the classical Navier-Stokes theory is inadequate. An excellent review of micropolar fluids and their applications was presented by Ariman *et al.* [21]. Several researchers have considered stretching sheet problems in micropolar fluids including the papers of Ishak *et al.* [22; 23]. Available literature on convective flow over a stretching sheet shows that the combined effect of the unsteadiness and the thermal buoyancy has not been investigated for micropolar fluids.

Motivated by these applications, in the present paper we explore the effects of thermal buoyancy on an unsteady boundary layer flow and heat transfer induced by a vertical stretching sheet immersed in a micropolar fluid. In contrast to the work of Kumari *et al.* [18], the present work considers the effect of non-Newtonian fluid viz., micropolar model which includes Newtonian fluid as a special case. Further, the surface velocity is assumed to vary linearly with the distance along the sheet, whereas the temperature distribution at the surface is assumed to be constant. Because of the complexity and non-linearity of our problem, the transformed governing parabolic partial differential equations in two variables are solved numerically using the Keller-box method for various values of the physical parameters. The obtained numerical results are presented graphically for the velocity, the microrotation, and the temperature distribution; whereas the skin friction, the couple stress coefficient and the Nusselt number are presented in tables for different values of the pertinent parameters. For special cases, our results are found to be in good agreement with those of the results available in the literature (Grubka and Bobba [4], Ali [5], Ishak *et al.* [29] and Prasad *et al.* [30]). Moreover, the results obtained for the flow and heat transfer characteristics reveal many interesting behaviors that warrant further study on the micropolar flow phenomena.

## 2. Mathematical formulation of the problem

Consider an unsteady two-dimensional, laminar, free convection flow of an incompressible micropolar fluid at a vertical stretching sheet. The Cartesian coordinate system has its origin located at the leading edge of the sheet with the positive  $x$ -axis extending along the sheet in the upwards direction, while the  $y$ -axis is measured normal to the surface of the sheet and is positive in the direction from the sheet to the fluid. We assume that for time  $t < 0$  the fluid flow and heat transfer are at steady state. The unsteady fluid flow and heat transfer start at  $t = 0$ , the sheet is being stretched with the velocity  $u_w(x, t)$  along the  $x$ -axis, keeping the origin fixed. The thermo-physical properties of the sheet and the ambient fluid are assumed to be constant except the variation of density with temperature in the buoyancy force term. Under these assumptions (with the Boussinesq and boundary layer approximations), the governing equations for the convective flow and heat transfer of the viscous micropolar fluid are

$$\frac{\partial u}{\partial x} + \frac{\partial v}{\partial y} = 0, \quad (2.1)$$

$$\rho \left( \frac{\partial u}{\partial \bar{t}} + u \frac{\partial u}{\partial x} + v \frac{\partial u}{\partial y} \right) = (\mu + k) \frac{\partial^2 u}{\partial y^2} + k \frac{\partial \sigma}{\partial y} + \rho g \beta (T - T_\infty), \quad (2.2)$$

$$\rho j \left( \frac{\partial \sigma}{\partial \bar{t}} + u \frac{\partial \sigma}{\partial x} + v \frac{\partial \sigma}{\partial y} \right) = \gamma \frac{\partial^2 \sigma}{\partial y^2} - k \left( \frac{\partial u}{\partial y} + 2\sigma \right), \quad (2.3)$$

$$\rho C_p \left( \frac{\partial T}{\partial \bar{t}} + u \frac{\partial T}{\partial x} + v \frac{\partial T}{\partial y} \right) = \alpha_c \left( \frac{\partial T}{\partial x} \frac{\partial \sigma}{\partial y} - \frac{\partial T}{\partial y} \frac{\partial \sigma}{\partial x} \right) + K_c \frac{\partial^2 T}{\partial y^2}. \quad (2.4)$$

The appropriate initial and the boundary conditions for the problem are

$$u(x, y, 0) = u_i(x, y), \quad v(x, y, 0) = v_i(x, y), \quad \sigma(x, y, 0) = \sigma_i(x, y), \quad T(x, y, 0) = T_i(x, y), \quad (2.5)$$

$$u(x, 0, \bar{t}) = u_w(x, \bar{t}), \quad v(x, 0, \bar{t}) = 0, \quad \sigma(x, 0, \bar{t}) = -n \frac{\partial u}{\partial y}(x, \bar{t}), \quad T(x, 0, \bar{t}) = T_w(x, \bar{t}), \quad (2.6)$$

$$u(x, \infty, \bar{t}) = 0, \quad \sigma(x, \infty, \bar{t}) = 0, \quad T(x, \infty, \bar{t}) = T_\infty.$$

Here  $x$  and  $y$  are measured along and perpendicular to the sheet,  $\bar{t}$  is the dimensionless time,  $u$  and  $v$  are the velocity components along the  $x$  and  $y$  directions,  $\sigma$  is the microrotation component perpendicular to the  $xy$ -plane,  $T$  is the temperature,  $g$  is the acceleration due to gravity,  $\beta$  is the coefficient of thermal expansion,  $\rho$  is the density,  $j$  is the microinertia density,  $\mu$ ,  $k$  and  $\gamma$  are, respectively, the kinematic viscosity, the rotational viscosity and gyroviscosity of the fluid,  $C_p$  is the specific heat at constant pressure,  $K_c$  is the thermal conductivity,  $\alpha_c$  is the heat conductivity of the micropolar fluid, the subscripts  $i$ ,  $w$  and  $\infty$  denote respectively, the initial condition, the condition at the wall and the condition at the free stream. The last term in right hand side of Eq.(2.2) is due to the buoyancy force.

In the literature, we see authors imposing various types of boundary conditions on the microrotation vector fields. For example, some authors have imposed the condition of zero spin on the surface i.e.  $\sigma = 0$  which has the physical interpretation that there is a fluid solid interface with interactions so strong that the microstructure does not rotate relative to the surface. Some authors used  $n=0$  which corresponds to strong concentration of the microelements near the boundary. The case  $n=1/2$  indicates the vanishing of the antisymmetric part of the stress tensor which denotes weak concentration. The case  $n=1$  is used for modeling of turbulent boundary layer flows. Also, many authors have assumed  $\gamma = (\mu + k/2)j$  i.e.,  $\gamma/j\mu = 1 + k/2\mu$ , which predicts the correct behavior in the limiting case when the microstructure effects become negligible and the rotational spin  $\sigma$  reduces to the angular velocity of the fluid (see for details Ahmadi [24], Kline [25]).

We now introduce the following dimensionless variables

$$\eta = (C/\nu)^{1/2} y, \quad t = C\bar{t}, \quad \nu = \mu/\rho, \quad u_w(x,t) = u_s(x)P(t), \quad u_s(x) = Cx,$$

$$C = (du_w/dx)_{t=0}, \quad \psi = (C\nu)^{1/2} x P(t)f(\eta,t), \quad u = \partial\psi/\partial y, \quad v = -\partial\psi/\partial x,$$

$$\sigma = C(C/\nu)^{1/2} xP(t)H(\eta,t), \quad T - T_\infty = (T_w - T_\infty)G(\eta,t), \quad \text{Re}_x = Cx^2/\nu,$$

$$\text{Gr}_x = (T_w - T_\infty)x^3/\nu^2, \quad \lambda = \text{Gr}_x/\text{Re}_x^2 = g\beta(T_w - T_\infty)/C^2x$$

where  $\text{Re}_x$  is the local Reynolds number,  $\text{Gr}_x$  is the local Grashof number,  $\lambda$  is the buoyancy parameter (ratio of local Grashof number and local Reynolds number),  $\text{Pr} = \mu C_p / K_c$  is the Prandtl number; and  $K = k/\mu$ ,  $l = l = k/\rho j C$  and  $\alpha = C\alpha_c / \mu C_p$  are the three micropolar fluid parameters and  $\psi$  is the stream function defined in the usual way as  $u = \partial\psi/\partial y$ ,  $v = -\partial\psi/\partial x$ , and identically satisfy Eq.(2.1).

Using the above dimensionless variables Eqs (2.2), (2.3) and (2.4) can be written as

$$(1+K)f''' + Pf'' - Pf'^2 - P^{-1}P'f' - f_t' + KH' + P^{-1}\lambda G = 0, \quad (2.7)$$

$$(1+K/2)H'' + P(f'H' - f'H) - P^{-1}P_tH - H_t - l(2H + f'') = 0. \quad (2.8)$$

$$\text{Pr}^{-1}G'' + Pf'G' - G_t - \alpha PHG' = 0. \quad (2.9)$$

The corresponding boundary conditions (2.5) can be written as

$$f(0,t) = 0, \quad f'(0,t) = 1, \quad H(0,t) = -nf''(0,t), \quad G(0,t) = 1,$$

$$f'(\infty,t) = 0, \quad H(\infty,t) = 0, \quad G(\infty,t) = 0 \quad (2.10)$$

where the function  $P(t)$  characterizes the unsteadiness in the flow field due to the variation of the moving sheet with time. Here, the prime denotes derivatives with respect to  $\eta$ , and the subscript  $t$  denotes the partial derivatives with respect to  $t$ .

The parameter  $K$  depends on the shape and concentration of the microelements. The parameter  $l$  can be thought of as the fluid properties depending on the relative size of microstructure in relation to a geometrical length, and  $\alpha$  is the dimensionless heat conduction coefficient of the micropolar fluid. From the engineering point of view, the most important characteristics of the flow are the wall shear stress  $\tau_w$ , the wall couple stress  $M_w$  and the local rate of heat transfer from the wall  $q_w$ . Thus, our task is to investigate how the non-dimensional parameters influence these physical quantities.

These physical quantities are defined as

$$\tau_w = (\mu + K)(\partial u / \partial y)_{\text{at } y=0} + K(\sigma)_{\text{at } y=0}, \quad M_w = \gamma(\partial \sigma / \partial y)_{\text{at } y=0} + \alpha_c(\partial T / \partial x)_{\text{at } y=0},$$

$$q_w = \left[ K_c(\partial T / \partial y)_{\text{at } y=0} + \beta_c(\partial \sigma / \partial x)_{\text{at } y=0} \right]$$

where  $\beta_C$  is the thermal conductivity of the micropolar fluid. In terms of functions defining velocity, microrotation rate and temperature, the skin friction coefficient  $\tau_w$ , the wall couple stress coefficient  $M_w$  and the local Nusselt number  $q_w$  may be written as

$$\frac{\sqrt{R_x} T_w}{1 + (1 - n)K} = f''(0, t)P(t), \quad \frac{2R_x M_w \ell}{K(K + 2)} = H'(0, t)P(t), \quad \frac{N_w}{\sqrt{R_x}} = -G'(0, t) + N n f''(0, t)P(t)$$

where  $N_w = \frac{xq_w}{K_C(T_w - T_\infty)}$  (local Nusselt number) and  $N = \frac{C\beta_C}{K_C(T_w - T_\infty)}$  (heat conduction coefficient for a micropolar fluid).

### 3. Exact solutions for some special cases

Here, we present exact solutions in certain special cases. Such solutions are useful and serve as a baseline for comparison with the solutions obtained via numerical schemes. For a Newtonian fluid  $K = l = \alpha = 0$  and no microrotation, i.e.,  $H = 0$ , the equations reduce to those of Kumari *et al.* [18]. Further, for a steady case, i.e., when  $P = 1$  and when no free convection effects are considered, heat transfer degenerates: in this case the solutions for the velocity field and the temperature field are exactly similar to those of Gupta and Gupta [2] and Chen and Char [3]. In particular, the steady-state equations are obtained from Eqs (2.7) to (2.9) by substituting  $t = 0, P = 1, P_t = f'_t = G_t = H_t = 0$ : The equations are

$$(1 + K)f''' + f f'' - f'^2 + KH' + \lambda G = 0, \tag{3.1}$$

$$(1 + K/2)H'' + (f H' - f' H) - l(2H + f'') = 0, \tag{3.2}$$

$$\text{Pr}^{-1} G'' + f G' - H G = 0, \tag{3.3}$$

with boundary conditions

$$f(0) = 0, \quad f'(0) = 1, \quad H(0) = -n f''(0), \quad G(0) = 1, \tag{3.4}$$

$$f'(\infty) = 0, \quad H(\infty) = 0, \quad G(\infty) = 0.$$

Equations (2.7) to (2.9) under the boundary conditions (2.10) and initial conditions (2.11) to (2.14) have been solved numerically using the Keller-box method. It should be noticed that the velocity distributions of the stretching sheet representing the accelerating and decelerating flows were studied. They were respectively given by  $P(t) = 1 + At^2$  and  $P(t) = 1 - At^2$ .

#### 4. Numerical procedure

Equations (2.7) to (2.9) are highly non-linear, coupled partial differential equations. Exact analytical solutions are not possible for the complete set of equations subject to the boundary conditions (2.10). Hence we use an efficient implicit finite difference scheme for the solution process. The implicit finite difference scheme (see for details Cebeci and Bradshaw [26], Keller [27], and Vajravelu and Prasad [28]) is chosen for this purpose because it has been proven to be more than adequate to give accurate results for coupled boundary value problems. The coupled boundary value problems of third order in  $f$ , second order in  $H$  and second order in  $G$ , are reduced to a system of seven simultaneous differential equations of first order with respect to  $\eta$  by assuming  $f = f_1, f' = f_2, f'' = f_3, H = H_1, H' = H_2, G = G_1$  and  $G' = G_2$ . Initially, all first order derivatives with respect to  $\xi$  are replaced by two-point backward difference formulae of the form

$$\frac{\partial f}{\partial t} = \frac{(f)_i^{j+1/2} - (f)_{i-1}^{j+1/2}}{\Delta t}; \quad (f)_i^{j+1/2} = \frac{1}{2}(f_i^{j+1} + f_i^j), \quad \text{and} \quad f_i^j \approx f(i\Delta\eta, j\Delta t)$$

denote approximate values of  $f$  at the grid point  $(i\Delta\eta, j\Delta t)$ . To solve this system of equations we require five initial conditions; whilst we have only two initial conditions  $f(0, t), f'(0, t)$  on  $f$ , one initial condition  $H(0, t)$  on  $H$  and one initial condition on  $G(\xi, 0)$  on  $G$ . The other three initial conditions  $f''(0, t), H'(0, t)$  and  $G'(0, t)$  are not prescribed; however, the values of  $f'(\eta, t), H(\eta, t)$  and  $G(\eta, t)$  are known for  $\eta$  at infinity. Hence, we employ the Keller-box numerical scheme where these three boundary conditions are utilized to produce three unknown initial conditions at  $\eta = 0$ . To select  $\eta_\infty$ , we begin with some initial guess value and solve the boundary value problem for a set of parameters to obtain  $f''(0, t), H'(0, t)$  and  $G'(0, t)$ . Thus we start with the initial approximation as  $f_3(0, t) = \alpha_0, H_2(\xi, 0) = \beta_0$  and  $G_2(\xi, 0) = \gamma_0$  and then let  $\alpha_{11}, \beta_{11}$  and  $\gamma_{11}$  be the correct values of  $f_3(0, t), H_2(0, t)$  and  $G_2(0, t)$  respectively. We integrate the resulting system of seven differential equations using the fourth order Runge-Kutta method and obtain the values of  $f_3(0, t), H_2(0, t)$  and  $G_2(0, t)$ . Finally the problem has been solved numerically using a second order finite difference scheme known as the Keller-box method. The solution process is repeated with another larger value of  $\eta_\infty$  until two successive values of  $f''(0, t), H'(0, t)$  and  $G'(0, t)$  agree up to the desired decimal level signifying the limit of the boundary along  $\eta$ . The last value of  $\eta_\infty$  is chosen as appropriate value for that set of parameters.

The numerical solutions are obtained in four steps as follows:

- Reduce Eqs (2.7) to (2.9) to a system of first-order equations;
- Write the difference equations using central differences;
- Linearize the algebraic equations by Newton's method, and write them in a matrix-vector form; and
- Solve the linear system by the block tri-diagonal elimination technique.

For each value of  $t$  we get a set of algebraic equations: with each of the non-linear terms evaluated at the previous iteration, the algebraic equations are solved with iteration by the well-known Thomas algorithm. This process is repeated for the next  $t$  value and the problem is solved line by line until the desired  $t$  value is reached. For the sake of brevity the details of the solution process are not presented here.

It is also important to note that the computational time for each set of input parameters should be as short as possible. The physical domain in this problem is unbounded, whereas the computational domain has to be finite, we apply the far field boundary conditions for the pseudo-similarity variable at finite value denoted by  $\eta_{\max}$ . We ran our bulk of computations with  $\eta_{\max} = 7$ , which is sufficient to achieve asymptotically the far field boundary conditions for all values of the parameters considered. For numerical

calculations, a uniform step size of  $\Delta\eta = 0.005$  and  $\Delta t = 0.001$  are found to be satisfactory and the solutions are obtained with an error tolerance of  $10^{-6}$  in all the cases. To assess the accuracy of the present method, comparisons of the wall-temperature gradient between the present results and the previously published results are presented, for several special cases in Tab.1.

Table 1. Comparison of the values of the wall-temperature gradient  $-G'(0)$  obtained by Grubka and Bobba [3], Ali [5], Ishak *et al.* [29] and Prasad *et al.* [30] with the present results in the absence of microrotation when  $K = l = \alpha = \lambda = 0$  for  $n = 0.5$ .

Pr	Grubka and Bobba [4]	Ali [5]	Ishak <i>et al.</i> [29]	Prasad <i>et al.</i> [30]	Present results
0.01	-0.0099	****	-0.0099	-0.01017936	-0.01018
0.72	-0.4631	-0.4617	-0.4631	-0.4631462	-0.4630462
1.0	-0.5820	-0.5801	-0.5820	-0.5826707	-0.5826407
3.0	-1.1652	-1.1599	-1.1652	-1.16517091	-1.16513091
10.0	-2.3080	-2.2960	-2.3080	-2.308029	-2.308019
100.0	-7.7657	****	-7.7657	-7.769667	-7.769657

## 5. Results and discussion

Numerical computations are carried out to obtain the results for the convective boundary layer flow and heat transfer induced by a vertical stretching sheet immersed in a micropolar fluid. The present study involves three more parameters in addition to the usual Prandtl number, namely, the micropolar fluid parameters, the unsteady parameter and the buoyancy parameter. In order to get a clear insight into the physical problem, the velocity, microrotation and the temperature profiles are presented graphically in Figs 1-3. Values of the skin friction, the wall couples stress coefficient and the Nusselt number for different values of the physical parameters are recorded in Tab.2. In the present paper we have also considered two cases of unsteadiness, namely: accelerating and decelerating cases.

Figures 1a and 1b illustrate the effects of the material parameter and the buoyancy parameter on the horizontal velocity profile  $f'(\eta)$  for different values of unsteady parameter. It is noticed from the figures that  $f'(\eta)$  decreases and tends to zero as the distance increases from the boundary. The effect of increasing values of the buoyancy parameter  $\lambda$  and the material parameter  $K$  is to increase the velocity  $f'(\eta)$  and hence increases the boundary layer thickness. The velocity gradient at the surface  $|f''(0,t)|$  decreases as  $K$  increases. Thus, micropolar fluids show drag reduction compared to viscous fluids. Physically,  $\lambda > 0$  means heating of the fluid or cooling of the surface (assisting flow);  $\lambda < 0$  means cooling of the fluid or heating of the surface (opposing flow) and  $\lambda = 0$  means the absence of free convection currents (forced convection flow). Also, an increase in the value of  $\lambda$  can lead to an increase in the temperature difference  $(T_w - T_\infty)$ : This leads to an enhancement of the velocity  $f'(\eta)$  due to the enhanced convection currents and thus an increase in the boundary layer thickness. This is true for both steady and unsteady cases. The influence of the unsteady parameter is to decrease the velocity  $f'(\eta)$ : this is due to the fact that the velocity gradient at the surface is larger for larger values of  $t$  which produces the larger skin friction coefficient and hence boundary layer thickness decreases.

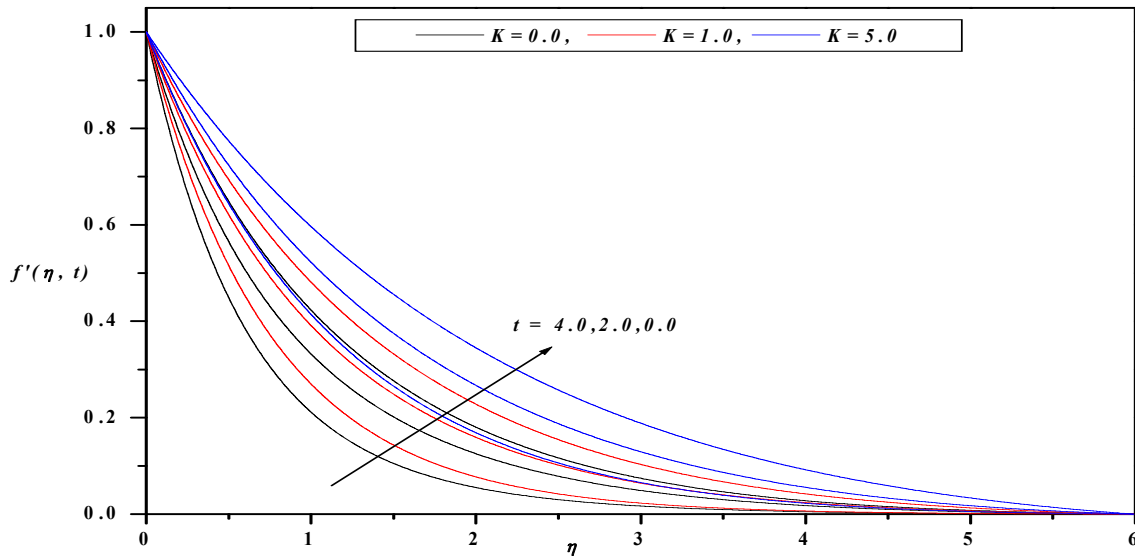


Fig.1a. Horizontal velocity profiles for different values of  $t$  and  $K$  with  $n=0.5$ ,  $Pr=0.72$ ,  $\alpha=0.1$ ,  $l=0.5$ ,  $a=0.1$ ,  $\lambda=0.2$ .

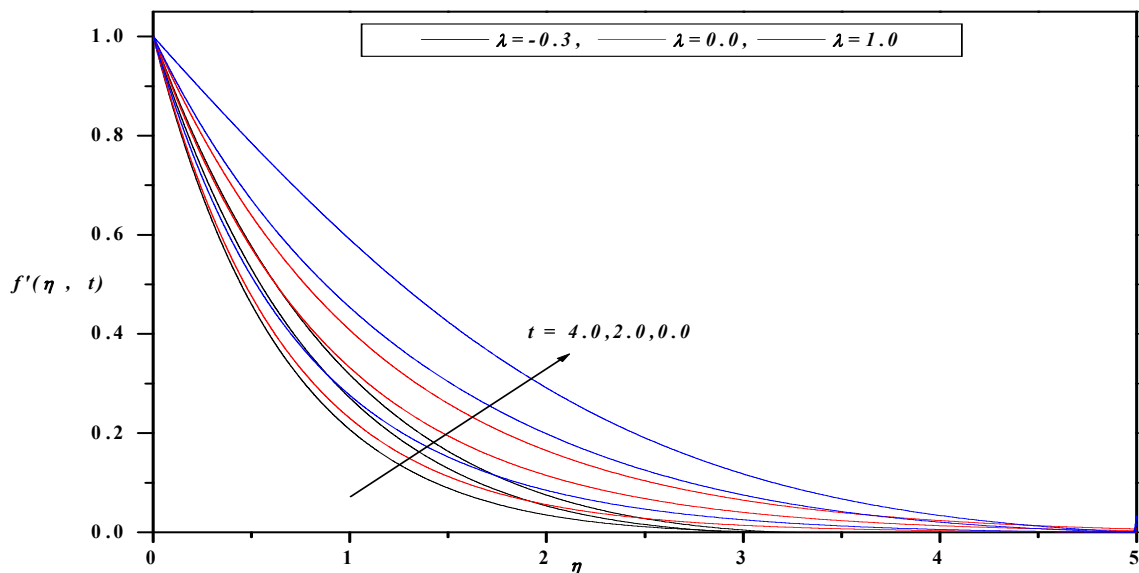


Fig.1b. Horizontal velocity profiles for different values of  $t$  and  $\lambda$  with  $n=0.5$ ,  $Pr=0.72$ ,  $\alpha=0.1$ ,  $l=0.5$ ,  $a=0.1$ ,  $K=0.5$ .

Temperature profiles  $G(\eta)$  are shown graphically in Figs 2a to 2d for different values of the pertinent parameters. The general trend is that the temperature distribution is unity at the wall and with the changes in the physical parameters tends asymptotically to zero in the free stream region. The general trend from Figs 2a to 2d is that the effect of increasing values of the unsteady parameter is to decrease the temperature field and hence reduces the thermal boundary layer thickness as compared to those of steady case shown graphically in Figs 2a-2d. Also, these figures show the effect of the unsteady parameter and the material parameters, namely:  $K$  and  $\alpha$  on the temperature  $G(\eta)$ . The effect of increasing values of the material parameters is to decrease the temperature distribution in the flow region. This is in conformity with the fact that an increase in the material parameters leads to decrease in the thermal boundary layer thickness.

This is true even for non-zero values of the unsteady parameter shown graphically in Figs 2a-2b. Figure 2c depicts the effect of the buoyancy parameter on the temperature profile  $G(\eta)$  for different values of the unsteady parameter. From the graphical presentation, it can be observed that an increase in the value of the buoyancy parameter  $\lambda$  results in a decrease in the thermal boundary layer thickness and this results in an increase in the magnitude of the wall temperature gradient (see Tab.2). This in turn produces an increase in the surface heat transfer rate. The variations of  $G(\eta)$  for different values of the Prandtl number  $Pr$  and the unsteadiness are displayed in Fig.2d. The effect of increasing values of the Prandtl number  $Pr$  is to decrease the temperature  $G(\eta)$ . That is, an increase in the Prandtl number  $Pr$  means a decrease in the thermal conductivity and hence decreases of thermal boundary layer thickness. This can be even noticeable for zero and non-zero values of  $t$ .

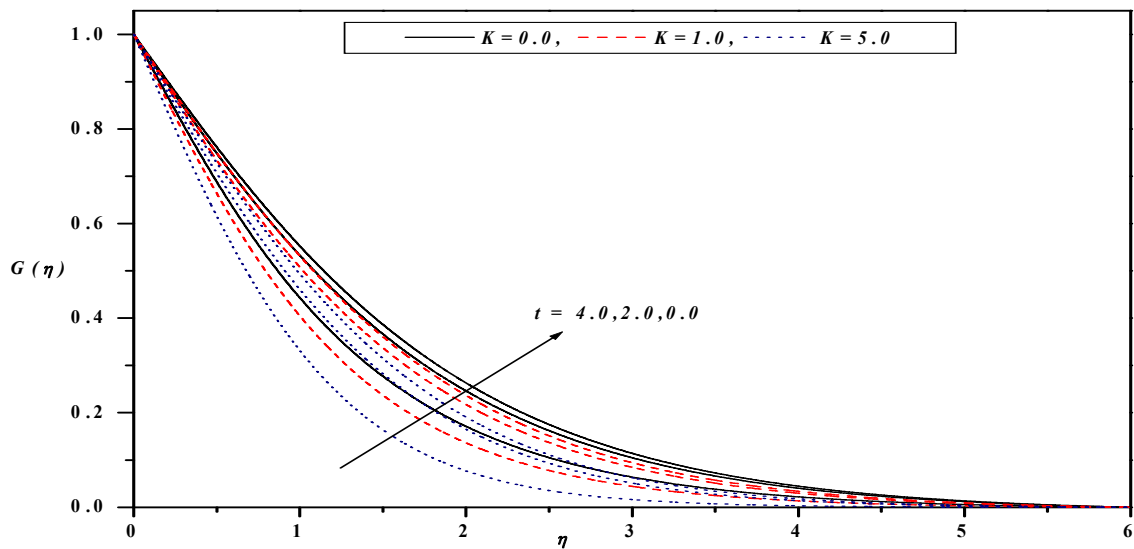


Fig.2a. Temperature profiles for different values of  $t$  and  $K$  with  $n=0.5$ ,  $Pr=0.72$ ,  $\alpha=0.1$ ,  $l=0.5$ ,  $a=0.1$ ,  $\lambda=0.2$ .

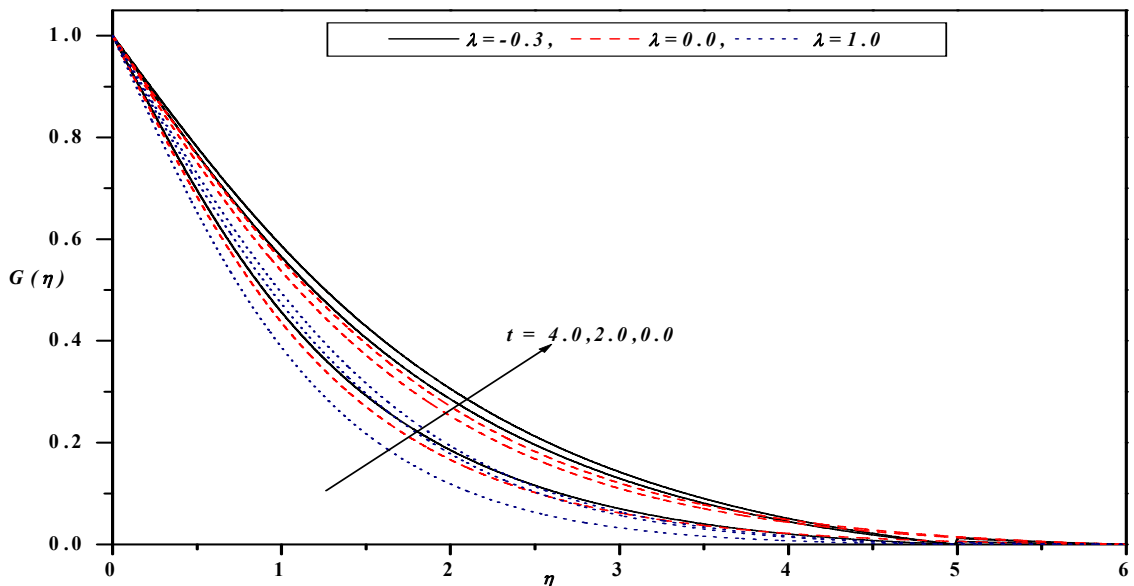


Fig.2b. Temperature profiles for different values of  $t$  and  $\lambda$  with  $n=0.5$ ,  $Pr=0.72$ ,  $\alpha=0.1$ ,  $l=0.5$ ,  $a=0.1$ ,  $K=0.5$ .

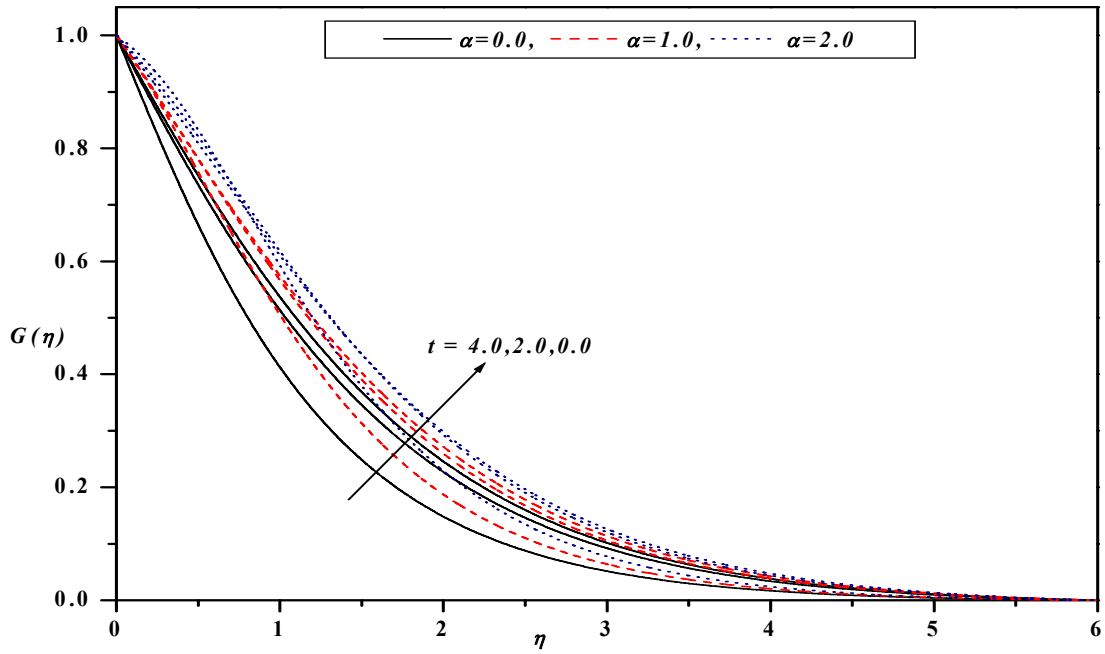


Fig.2c. Temperature profiles for different values of  $t$  and  $\alpha$  with  $n=0.5$ ,  $Pr=0.72$ ,  $\lambda=0.2$ ,  $l=0.5$ ,  $a=0.1$ ,  $K=0.5$ .

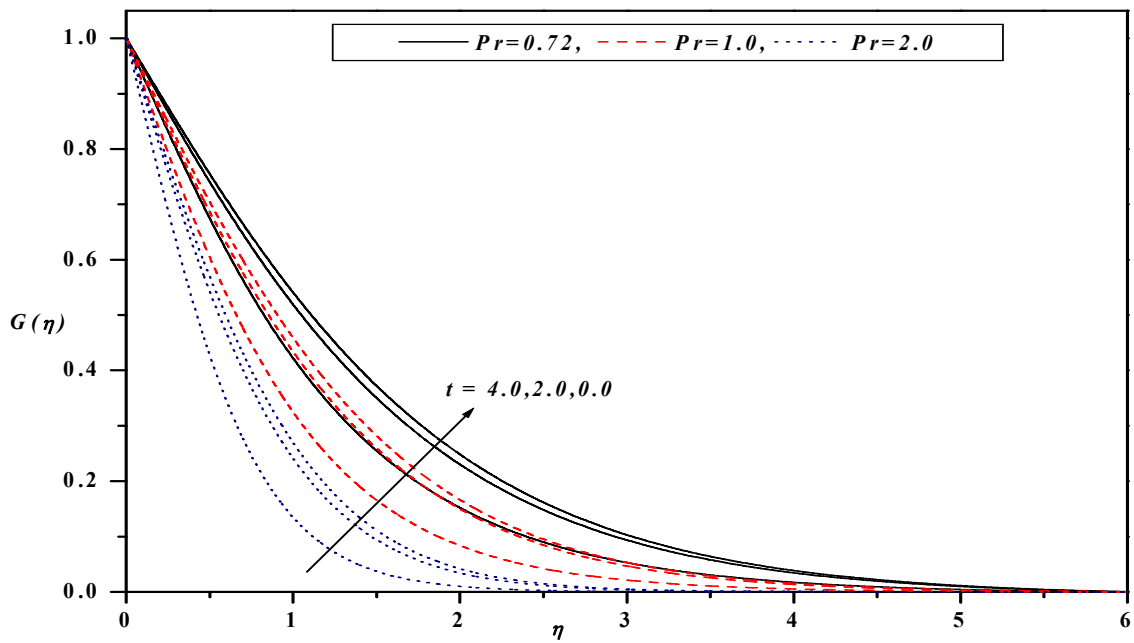


Fig.2d. Temperature profiles for different values of  $t$  and  $Pr$  with  $n=0.5$ ,  $Pr=0.72$ ,  $\lambda=0.2$ ,  $l=0.5$ ,  $\beta=0.1$ ,  $a=0.1$ ,  $K=0.5$ .

Table 2. Values of  $f''(0,t)$ ,  $G'(0,t)$  and  $H'(0,t)$  for different values of the physical parameters.

A	Pr	$\lambda$	$\alpha$	n	I	K	t=0			t=2.0			t=4.0		
							$f''(0,t)$	$G'(0,t)$	$H'(0,t)$	$f''(0,t)$	$G'(0,t)$	$H'(0,t)$	$f''(0,t)$	$G'(0,t)$	$H'(0,t)$
							0.0	-0.8472	-0.4863	-0.4342	-1.1801	-0.5138	-0.6809	-1.6410	-0.6420
0.5	-0.7939	-0.5001	-0.3520	-1.0571	-0.5308	-0.5426	-1.4664	-0.6720	-1.0344						
1.0	-0.7332	-0.5112	-0.2963	-0.9672	-0.5447	-0.4515	-1.3386	-0.6968	-0.8605						
5.0	-0.5077	-0.5567	-0.1335	-0.6464	-0.6035	-0.1951	-0.8801	-0.8047	-0.3686						
0.0	-0.7963	-0.5006	-0.3674	-1.0656	-0.5326	-0.6518	-1.4727	-0.6758	-1.1519						
1.0	-0.7931	-0.4999	-0.3463	-1.0513	-0.5296	-0.4544	-1.4617	-0.6692	-0.9333						
2.0	-0.7924	-0.4998	-0.3407	-1.0434	-0.5278	-0.3092	-1.4545	-0.6651	-0.7579						
0.5	-0.7939	-0.5001	-0.3520	-1.0571	-0.5308	-0.5426	-1.4664	-0.6720	-1.0344						
1.0	-0.8893	-0.4790	-0.9843	-1.1738	-0.5006	-1.4275	-1.6257	-0.6038	-2.5111						
0.0	-0.7944	-0.5096	-0.3522	-1.0574	-0.5466	-0.5428	-1.4668	-0.7115	-1.0345						
1.0	-0.7897	-0.4214	-0.3504	-1.0574	-0.4050	-0.5414	-1.4635	-0.3906	-1.0332						
2.0	-0.7853	-0.3466	-0.3487	-1.0496	-0.2956	-0.5402	-1.4606	-0.2021	-1.0321						
0.0	-1.0682	-0.4458	-0.4738	-1.2419	-0.4753	-0.6056	-1.5454	-0.6259	-1.0667						
-0.3	-0.8954	-0.4790	-0.4001	-1.1255	-0.5092	-0.5687	-1.4961	-0.6534	-1.0478						
0.0	-0.4453	-0.5569	-0.1668	-0.8219	-0.5883	-0.4350	-1.3622	-0.7199	-0.9790						
1.0	-0.7939	-0.5001	-0.3520	-1.0571	-0.5308	-0.5426	-1.4664	-0.6720	-1.0344						
0.72	-0.8053	-0.6078	-0.3559	-1.0651	-0.6471	-0.5443	-1.4705	-0.8268	-1.0353						
1.0	-0.8272	-0.9098	-0.3652	-1.0802	-0.9720	-0.5483	-1.4775	-1.2476	-1.0374						
2.0	-0.7939	-0.5001	-0.352	1.7986	-0.4345	1.712	*****	*****	*****						
-0.2	-0.7939	-0.5001	-0.352	-0.7861	-0.4991	-0.2606	-0.7863	-0.4985	-0.2581						
0.0	-0.7939	-0.5001	-0.352	-1.6393	-0.6516	-1.3424	-2.7204	-1.1168	-3.6494						
0.5	-0.7939	-0.5001	-0.352												

The microrotation profiles  $H(\eta)$  are presented in Figs 3a-3d for different values of the governing parameters. The microrotation profiles are parabolic in nature for a fixed value of  $n = 0.5$  and continuously decreases with  $\eta$  and becomes zero far away from the plate, satisfying the boundary conditions (2.10). As expected, the microrotation effect is more dominant near the surface. Also, the microrotation decreases as  $K$  increases in the vicinity of the plate but the opposite is true away from the plate. This is true even for zero and non-zero values of  $t$  as shown in Fig.3a. The buoyancy parameter has the similar effect on the microrotation as those seen in temperature profiles and is shown graphically in Fig.3b. Figure 3c demonstrates the dependence of the micropolar fluid parameter  $l$ . The effect of the micropolar fluid parameter  $l$  is to enhance the thickness of the microrotation and hence the boundary layer thickness increases as  $l$  increases. Figure 3d elucidates the effect of  $n$  on the microrotation profile for different values of the unsteady parameter. The effect of  $n$  is to reduce the thickness of the microrotation and the thickness is smaller for  $n = 0.5$  when compared to  $n = 1.0$ . This is true even for all values of the unsteady parameter.

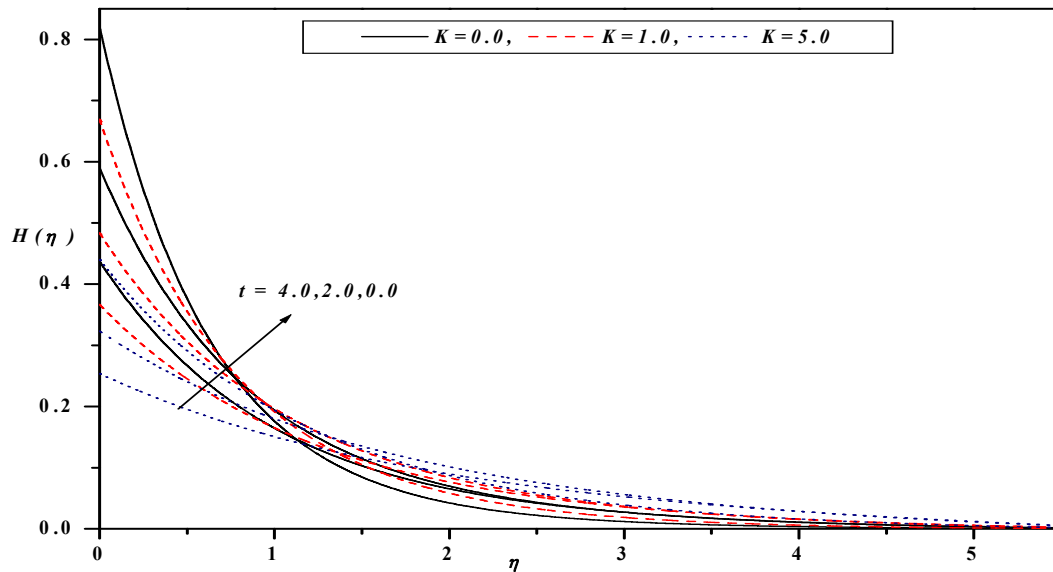


Fig.3a. Microrotation profiles for different values of  $t$  and  $K$  with  $n=0.5$ ,  $Pr=0.72$ ,  $\alpha=0.1$ ,  $l=0.5$ ,  $a=0.1$ ,  $\lambda=0.2$ .

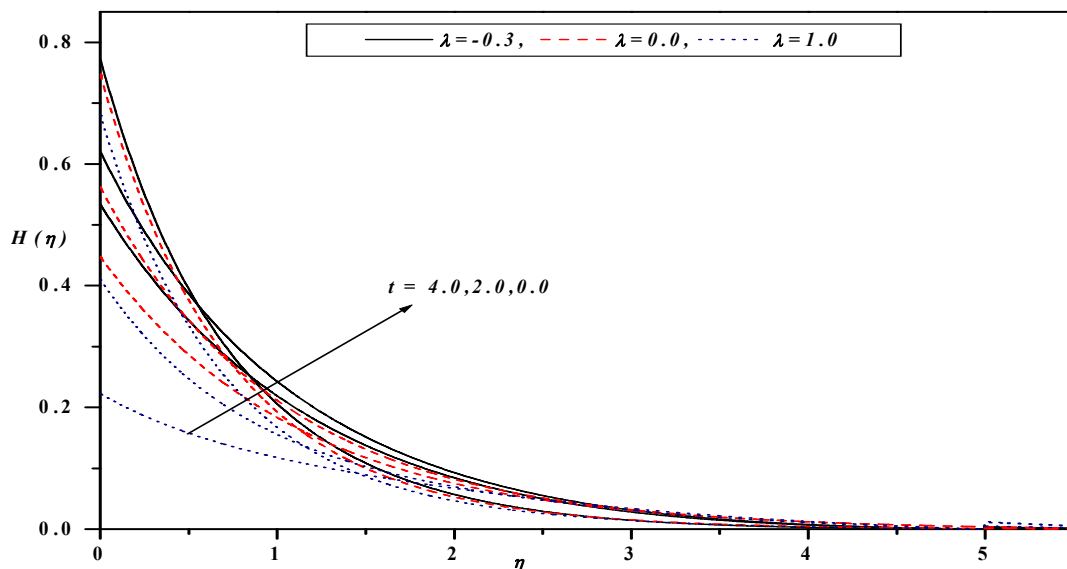


Fig.3b. Microrotation profiles for different values of  $t$  and  $\lambda$  with  $n=0.5$ ,  $Pr=0.72$ ,  $\alpha=0.1$ ,  $l=0.5$ ,  $a=0.1$ ,  $K=0.5$ .

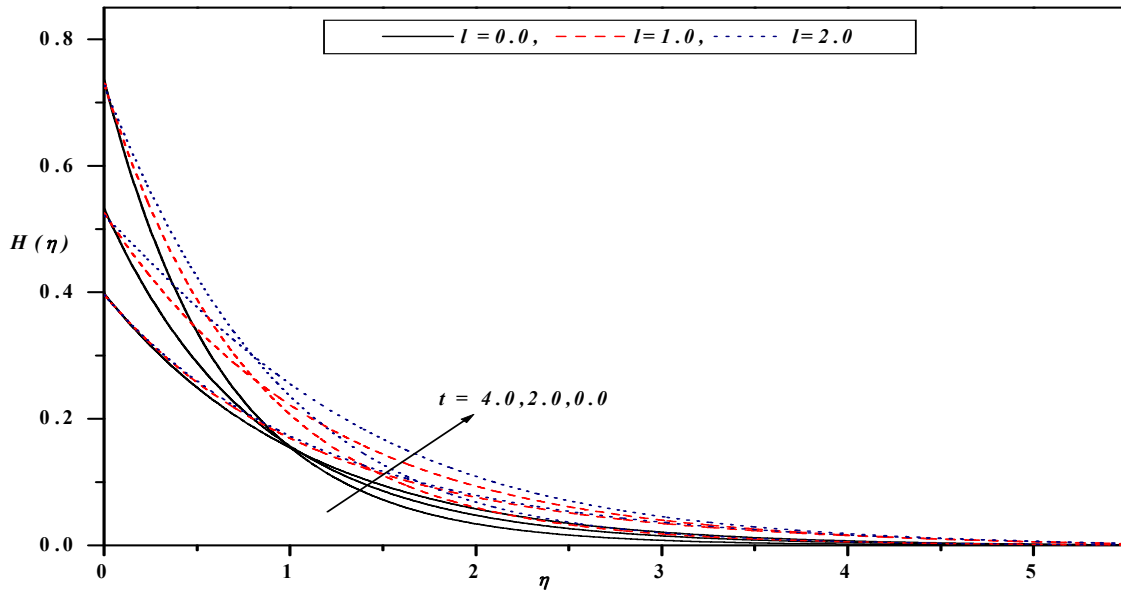


Fig.3c. Microrotation profiles for different values of  $t$  and  $l$  with  $n=0.5$ ,  $Pr=0.72$ ,  $\alpha=0.1$ ,  $\lambda=0.2$ ,  $a=0.1$ ,  $K=0.5$ .

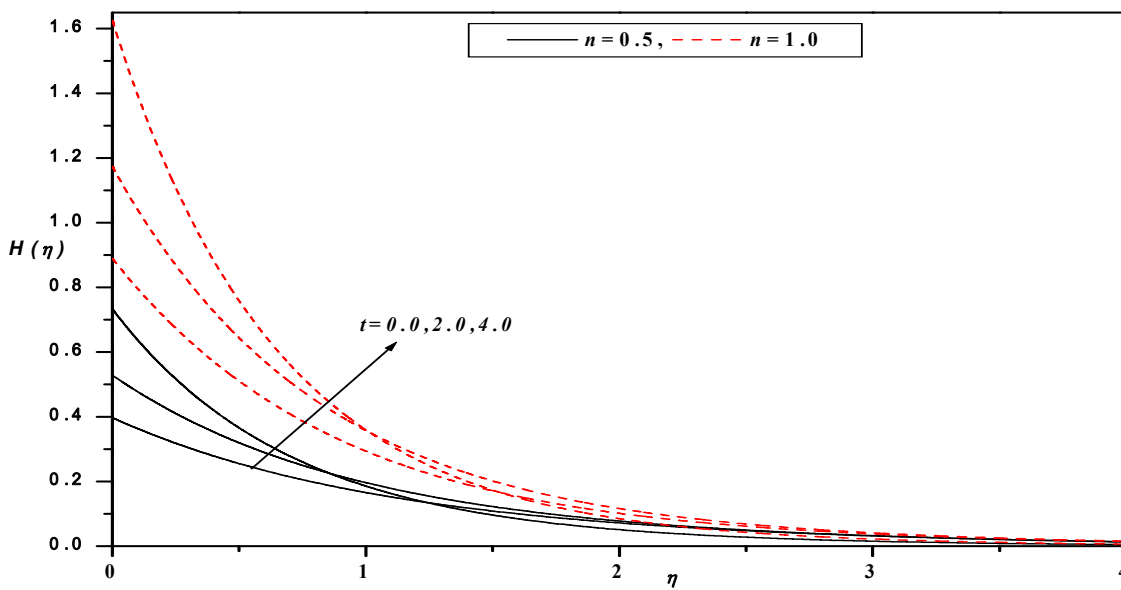


Fig.3d. Microrotation profiles for different values of  $t$  and  $n$  with  $l=0.5$ ,  $Pr=0.72$ ,  $\alpha=0.1$ ,  $\lambda=0.2$ ,  $a=0.1$ ,  $K=0.5$ .

Numerical results for the local skin friction coefficient and wall temperature gradient in terms of  $f''(0,0)$ ,  $H'(0,0)$  and  $G'(0,0)$  with changes in the physical parameters are recorded in Tab.2. The effect of  $K, l$  and  $\lambda$  is to decrease; whereas the effect of the unsteady parameter is to increase the magnitude of the surface velocity gradient  $|f''(0,0)|$  and the magnitude of the couple stress coefficient  $|H'(0,0)|$ . Thus,

micropolar fluids show drag reduction compared to viscous fluids. The effects of  $K, \lambda$  and  $Pr$  are to decrease and  $l$  is to enhance the wall temperature gradient  $|G'(0,0)|$ .

## 6. Conclusions

Some of the important findings of the study are as follows:

- The effect of increasing values of  $\lambda$  and  $K$  is to increase  $f'(\eta)$  and hence increases the boundary layer thickness. The velocity gradient at the surface  $|f''(0,t)|$  decreases as  $K$  increases. Thus, micropolar fluids show drag reduction compared to viscous fluids.
- The effect of increasing values of  $K$  is to decrease the temperature distribution in the flow region.
- The effect of  $\lambda$  results in a decrease in the thermal boundary layer thickness and this results in an increase in the magnitude of the wall temperature gradient (see Tab.2). This in turn produces an increase in the surface heat transfer rate.
- The microrotation effect is more dominant near the surface and decreases as  $K$  increases in the vicinity of the plate but the reverse happens away from the plate.
- Of all the parameters, the material parameters have the strongest effects on the drag, heat transfer characteristics, the horizontal velocity and the temperature fields.

## Acknowledgments

The authors appreciate the constructive comments of the reviewer which led to definite improvements in the paper. One of the authors (Hanumesh Vaidya) is thankful to the University Grants Commission, New Delhi, for supporting financial support under Minor Research Project (Grant No. MRP(S)-0060/12-13/KAUG062/UGC-SWRO)

## Nomenclature

- $A$  – non-dimensional micropolar parameters
- $C$  – positive constant
- $C_f$  – skin friction
- $C_p$  – specific heat at constant pressure
- $f$  – dimensionless stream function
- $Gr_x$  – local Grashof number
- $g$  – acceleration due to gravity
- $j$  – microinertia density
- $K$  – material parameter
- $K(T)$  – temperature dependent thermal conductivity
- $K_c$  – thermal conductivity
- $l$  – micropolar fluid parameter
- $M_w$  – wall couple stress
- $N$  – heat conduction coefficient
- $N_w$  – local Nusselt number
- $Pr$  – Prandtl number
- $q_w$  – local rate of heat transfer from the wall
- $Re_x$  – local Reynolds number
- $T$  – temperature
- $T_w$  – temperature of the plate
- $t$  – unsteady parameter

- $\bar{t}$  – dimensionless time  
 $u, v$  – velocity components in the  $x$  and  $y$  directions  
 $x, y$  – Cartesian coordinates  
 $\alpha$  – dimensionless heat conduction coefficient  
 $\alpha_C$  – heat conductivity  
 $\beta$  – thermal expansion coefficient  
 $\beta_C$  – thermal conductivity  
 $\gamma$  – gyroviscosity  
 $\eta$  – similarity variable  
 $\kappa$  – rotational viscosity  
 $\lambda$  – buoyancy or mixed convection parameter  
 $\mu$  – kinematic viscosity  
 $\nu$  – kinematic viscosity  
 $\rho$  – density  
 $\sigma$  – microrotation component  
 $\tau_w$  – wall shear stress  
 $\psi$  – stream function

### Superscript

- $'$  – differentiation with respect to  $\eta$

### Subscripts

- $t$  – partial derivative with respect to  $t$   
 $w$  – condition at the wall  
 $\infty$  – condition at infinity

### References

- [1] Crane L.J. (1970): *Flow past a stretching plate*. – ZAMP, vol.21, pp.645-647.  
 [2] Gupta P.S. and Gupta A.S. (1977): *Heat and mass transfer on a stretching sheet with suction or blowing*. – Can. J. Chem. Eng., vol.55, pp.744-746.  
 [3] Chen C.K. and Char M.I. (1988): *Heat transfer of a continuous stretching surface with suction or blowing*. – J. Math. Anal. Appl., vol.135, pp.568-580.  
 [4] Grubka L.G. and Bobba K.M. (1985): *Heat transfer characteristics of a continuous stretching surface with variable temperature*. – ASME J. Heat Transfer, vol.107, pp.248-250.  
 [5] Ali M.E. (1994): *Heat transfer characteristics of a continuous stretching surface*. – Heat Mass Transfer, vol.29, pp.227-234.  
 [6] Datta B.K., Roy P. and Gupta A.S. (1985): *Temperature field in the flow over a stretching sheet with uniform heat flux*. – Int. Comm. Heat Mass Transfer, vol.12, pp.89-94.  
 [7] Vajravelu K. (1994): *Flow and heat transfer in a saturated porous medium over a stretching surface*. – ZAMM, vol.74, pp.605-614.  
 [8] Chen T.S. and Strobel F.A. (1980): *Buoyancy effects in boundary layer adjacent to a continuous moving horizontal flat plate*. – ASME J. Heat Transfer, vol.102, pp.170-172.  
 [9] Moutsoglou A. and Chen T.S. (1980): *Buoyancy effects in boundary layers on inclined continuous moving sheets*. – ASME J. Heat Transfer, vol.102, pp.371-373.

- [10] Chen C.H. (1998): *Laminar mixed convection adjacent to vertical continuously stretching sheets*. – Heat and Mass Transfer, vol.33, pp.471-476.
- [11] Ingham D.B. (1986): *Singular and non-unique solutions of the boundary layer equations for the flow due to a free convection near a continuous moving vertical plate*. – ZAMP, vol.37, pp.559-572.
- [12] Ramachandran N., Armaly B.F. and Chen T.S. (1987): *Correlation for laminar mixed convection on boundary layers adjacent to inclined continuous moving sheets*. – Int. J. Heat Mass Transfer, vol.30, pp.2196-2199.
- [13] Lee S.L. and Tsai J.S. (1990): *Cooling of a continuous moving sheet of finite thickness in the presence of natural convection*. – Int. J. Heat Mass Transfer, vol.33, pp.457-464.
- [14] Vajravelu K. (1994): *Convection heat transfer at a stretching sheet with suction or blowing*. – J. Math. Anal. Anal., vol.188, pp.1002-1011.
- [15] Elbashbeshy E.M.A. and Bazid M.A.A. (2003): *Heat transfer over an unsteady stretching surface with internal heat generation*. – Appl Math and Comp., vol.138, pp.239-245.
- [16] Abd El-Aziz M. (2009): *Radiation effect on the flow and heat transfer over an unsteady stretching sheet*. – Int. Comm. Heat Mass Transfer, vol.36, pp.521-524.
- [17] Takhar H.S. and Nath G. (1998): *Unsteady flow over a stretching surface with a magnetic field in a rotating fluid*. – ZAMP, vol.49, pp.989-1001.
- [18] Kumari M., Slaouti A., Takhar H.S., Nakamura S. and Nath G. (1996): *Unsteady free convection flow over a continuous moving vertical surface*. – Acta Mechanica, vol.116, pp.75-82.
- [19] Eringen A.C. (1966): *Theory of micropolar fluids*. – J. Math. Mech., vol.16, pp.1-18.
- [20] Eringen A.C. (1972): *Theory of thermomicrofluids*. – J. Math. Anal. Appl., vol.38, pp.480-496.
- [21] Armin T., Turk M.A. and Sylvester N.D. (1974): *Application of microcontinuum fluid mechanics*. – Int. J. Engng. Sci., vol.12, pp.273-279.
- [22] Ishak A., Nazar R. and Pop I. (2008): *Heat transfer over a stretching surface with variable surface heat flux in micropolar fluids*. – Phys. Lett., vol.372, pp.559-561.
- [23] Ishak A., Nazar R. and Pop I. (2007): *Magnetohydrodynamic stagnation point flow towards a stretching vertical sheet in a micropolar fluid*. – Magnetohydrodynamics, vol.43, pp.83-97.
- [24] Ahmadi G. (1976): *Self-similar solution of incompressible micropolar boundary layer flow over a semi-infinite plate*. – Int. J. Engng. Sci., vol.14, pp.639.
- [25] Kline K.A. (1977): *A spin-vorticity relation for unidirectional plane flows of micropolar fluids*. – Int. J. Engng. Sci., vol.15, pp.131-134.
- [26] Cebeci T. and Bradshaw P. (1984): *Physical and Computational Aspects of Convective Heat Transfer*. – 1<sup>st</sup> ed., New York: Springer-Verlag.
- [27] Keller H.B. (1992): *Numerical Methods for Two-Point Boundary Value Problems*. – New York: Dover Publ.
- [28] Vajravelu K. and Prasad K.V. (2014): *Keller-box method and its application*. – HEP and Walter De Gruyter GmbH, Berlin/Boston.
- [29] Ishak A. (2010): *Thermal boundary layer flow over a stretching sheet in a micropolar fluid with radiation effect*. – Meccanica, vol.45, pp.367-373.
- [30] Prasad K.V., Sujatha A., Vajravelu K. and Pop I. (2010): *MHD flow and heat transfer of a UCM fluid over a stretching surface with variable thermophysical properties*. – Meccanica, vol.47, pp.1425-1439.

Received: August 3, 2015

Revised: January 3, 2016